Cryogenics 101 (2019) 111–124

Contents lists available at ScienceDirect

Cryogenics

journal homepage: www.elsevier.com/locate/cryogenics

Review article

Pressed copper and gold-plated copper contacts at low temperatures – A review of thermal contact resistance

R.C. Dhuley

Fermi National Accelerator Laboratory, Batavia, IL 60510, United States

A B S T R A C T

Cryogenic systems that use cryocoolers with conduction cooling for attaining temperatures of 4.2 K and below routinely employ mechanically pressed components of copper to form the heat conduction path. To aid the design of such systems, the present paper reviews thermal contact resistance data of pressed copper-copper and gold-plated copper-copper contacts from nearly twenty measurement programs that span across past fifty years. Relevant theoretical models of thermal contact resistance are briefly reviewed and compared with the experimental data. Gold-plated copper contacts display reasonable trend with the models, which may serve as a design reference for such contacts. A few measurement techniques are also summarized that enable quick characterization of thermal contacts at low temperatures.

1. Introduction

The topic of thermal contact resistance at cryogenic temperatures of 4 K and below touches a number of emerging areas- space based experiments involving sensitive detectors operating at sub-Kelvin temperatures (example [1]), ground based astrophysics experiments aiming to study dark matter [2] and dark energy, electronic packaging of superconducting circuits [3], apparatus for quantum information science [4], and virtually any cryogen-free system that is conductively cooled by closed-cycle cryocoolers. The thermal contact resistance controls the system's key features: a bad thermal contact can lead to long cooldown time, poor thermal equilibrium between the sample to be cooled and the cooler even when the heat leak into the sample is small, and large temperature step across the contact for small heat flows during operation. The latter diminishes the useful temperature range of sample operation even when the cooler is able to attain its expected base temperature. The problem worsens at lower temperatures because the thermal contact resistance typically grows faster than linear with decreasing temperature. The knowledge of thermal contact resistance is therefore crucial for an effective thermal design of a low temperature cryogenic system.

Mechanically pressed thermal joints allow for easy make and break, a feature not available with soldered, casted, or welded joints. Thermal contact resistance of mechanically pressed metallic joints has been widely studied for applications near room temperature. The literature has hundreds of papers that report experimental data, theoretical modeling, and topical reviews [5–9]. At cryogenic temperatures, especially 4 K and below, data are few and theoretical models are rare. Gmelin et al. [10] reviewed experimental thermal resistance data of pressed contacts of copper, stainless steel, brass, aluminum, and other alloys in the temperature range of 0.2–300 K. The use of various interposers or filler materials such as the metal indium, thermal greases, varnish, etc., was surveyed and the interposed contacts were found to possess lower thermal resistance than dry (bare) contacts. Although Gmelin et al. qualitatively discussed the effects of parameters such as the pressing force, surface roughness, and surface conditions (oxides, adsorbed gases, coatings), their review lacks a possible quantitative assessment with theoretical models. Woodcraft [11] commented on Gmelin et al.'s review that even clean dry metallic contacts pressed with a large force can produce thermal resistance as low as that of the interposed ones. Woodcraft argued further that at lowest (sub-Kelvin) temperatures dielectric interposers may themselves have large bulk thermal resistance and metallic fillers *viz.* indium and lead/tin-based solders will become superconducting. Both these effects will increase the overall thermal resistance across a contact. Therefore, Woodcraft recommended the use of clean, dry contacts pressed with a large force for sub-Kelvin applications. Mamiya et al.'s [12] review covered experimental electrical resistance data of dry and soldered metallic contacts developed for applications at 4.2 K and colder. Van Sciver et al. [13] compiled data of several types of contacts for use at cryogenic temperatures, including thermally conducting as well as thermally insulating contacts.

High purity copper and high purity aluminum are the only practical materials that offer large bulk thermal conductivity near 4 K and hence are typically used in cryogenic systems operating near this temperature. Below 1.2 K, aluminum becomes a superconductor and hence a poor thermal conductor. Therefore, copper is the only metal useful as a thermal conductor below 1 K. Although copper can provide significant bulk thermal conductance at lowest temperatures, cryogenic systems with pressed copper components can experience substantial thermal

E-mail address: rdhuley@fnal.gov.

https://doi.org/10.1016/j.cryogenics.2019.06.008
Received 28 March 2019; Received in revised form 8 June 2019; Accepted 17 June 2019
Available online 21 June 2019

Nomenclature

k	thermal conductivity [W/m K]
a	constriction spot size [m]
σ	mean surface roughness [m]
m	mean slope of asperities [rad]
R_C	thermal constriction resistance [K m^2/W]
A_a	surface area of apparent contact [m^2]
A_p	surface area of physical contact [m^2]
p_{app}	applied pressure [Pa]
H_c	surface microhardness [Pa]
E	modulus of elasticity [pa], heat carrier energy [j]
ν	Poisson's ratio [–]
q	heat flux [W/m^2]
T	temperature [K]
v	heat carrier velocity [m/s]
N	heat carrier density [1/m^3]
α	probability of interfacial transmission [–]
r	probability of interfacial reflection [–]
θ	heat carrier angle of incidence [rad]
μ	chemical potential [J]
R_{BD}	thermal boundary resistance [K m^2/W]
R_{BC}, R_{BCt}, R_c	total thermal contact resistance [K m^2/W]
C_v	Specific heat per unit volume [J/K m^3]
Z	the product vC_v
k_B	Boltzmann constant [m^2 kg/(s^2 K)]
n_e	conduction electron density [1/m^3]
l_e	conduction electron mean free path [m]
R_{BCe}	electrical contact resistance [Ω]
L_0	Lorenz number [W Ω/K^2]
ϕ	sample diameter [m]
H	heater [–]
L	inductance [H]
I	current [A]
V	voltage [V]
RRR	residual resistivity ratio [–]
DMM	diffuse mismatch model [–]
WF	Wiedemann-Franz law
F_{screw}	pressing force at a screw-fastened contact [N]
τ_{screw}	torque applied to a screw [N m]
μ_b, μ	coefficient of friction [-]
P	thread pitch of a screw [m]
d, d_h, d_k	mean diameter of a screw, screw head, clearance screw hole [m]
R_a	average surface roughness [m]
R_q	root mean square surface roughness [m]

Subscripts

s	equivalent
1, 2	entity 1, 2
$1 \rightarrow 2$	from entity 1 to 2
F	Fermi level
ref	reference

resistance at the copper-copper contacts. It is therefore vital to have sound knowledge of thermal contact resistance of copper-copper joints at low temperatures.

In the present work we review the data from nearly twenty experimental measurement programs on pressed bare copper-copper and gold-plated copper-copper joints at 4.2 K and below. Many of these data were measured for specific end-applications and hence may not be directly useful for designing new cryogenic systems. To aid the latter, we review some thermal contact resistance models and, after making reasonable assumptions, evaluate them with the literature data. Based on the fair trend seen between the data on gold-plated contacts and contact resistance models, we propose a case for thorough parametric characterization of gold-plated contacts that may generate a reference design guideline for future cryogenic systems. This review also discusses some techniques for quick thermal characterization of pressed copper contacts at cryogenic temperatures.

2. Theoretical models of thermal contact resistance

Pressed solids have physical contact at the microscopic surface asperities and heat is constricted to flow across these micro-asperity contacts. The literature has widely dealt with constriction thermal resistance at pressed contacts, which is the restriction to heat flow due to thinning of the heat flow channels at the contacting asperities [5–9]. The thermal constriction resistance problem has three components: (a) geometrical, which describe how two rough surfaces touch each other on the microscopic level at the surface asperities (b) mechanical, wherein the deformation of the contacting asperities is characterized based on surface hardness, material elastic modulus, and applied pressure, and (c) thermal, which solves the heat diffusion equation through the narrow contacting asperities. It is not the subject of this paper to review the theoretical aspects of these topics in detail but is to introduce some basics that will enable tackling the practical cases encountered in cryogenics. We will limit the discussion in this section only to cover: (a) conforming flat contacts (b) steady state heat flow (c) joints operating in vacuum (d) no filler materials and (e) negligible radiation heat transfer. All these conditions relate closely to cryogenic systems.

The other component of thermal contact resistance deals with the interaction of the heat carriers with the physical boundary of the contacting solids. This component may be insignificant for contacts at room temperature. Here, the mean free path of the heat carriers is small compared to the asperity size and the definition of thermal conductivity in the diffusion limit is valid. At cryogenic temperatures, the mean free path of the heat carriers can become comparable to the asperity size and there can occur ballistic transport or even scattering at the physical interface. This topic at low temperatures has been widely studied for contacts that have a dielectric on at least one side, wherein phonons transport heat across the interface [14–16]. The case of metal-metal contacts has received very limited attention [17,18]. We will therefore review in detail the metal-metal thermal boundary resistance model introduced by Gundrum et al. [18].

2.1. Thermal constriction resistance

The premise of determining constriction thermal resistance is to look at the heat flow through a circular contact as depicted in Fig. 1. If the region in the bulk of the solid is dimensionally very large compared to the contact size, then the thermal resistance of the contact is given by

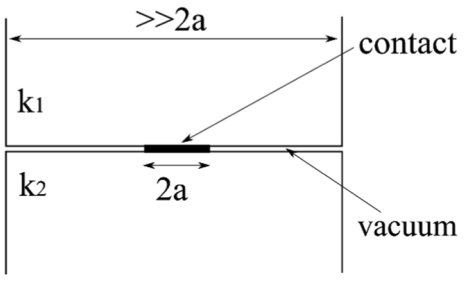

Fig. 1. Two solids with thermal conductivities k_1 and k_2, making contact over a circular region of radius a. The non-contacting region has vacuum.

[19]:

$$R_c = \frac{1}{4k_1 a} + \frac{1}{4k_2 a} = \frac{1}{2k_s a} \tag{1}$$

where k_1 and k_2 are bulk thermal conductivities, k_s is their harmonic mean (called the equivalent thermal conductivity), and a is radius of the contact spot. The model given by Eq. (1) is valid in the diffusion limit wherein the constriction size is much larger than the heat carrier mean free path.

Two pressed solids make physical contact in a complex way and their contact mechanics is defined in terms of the surface roughness parameter, σ and average slope of asperities, m of each surface. These parameters are schematized in Fig. 2. The surfaces prepared by standard machining processes tend to possess a Gaussian distribution of asperity heights (Ref. 16 in [8]). In this case $\sigma = R_q \approx \sqrt{\pi/2}R_a$, where R_q and R_a respectively are the RMS and average surface roughness. For a sampling length, L and asperity height distribution, $z(x)$ they are given by $R_a = (1/L)\int_0^{L_s} |z(x)|\, dx$ and $R_q = \sqrt{(1/L)\int_0^{L_s} z^2(x)dx}$, and can be obtained using a profilometer such as a laser scanning microscope. The distribution of asperity slopes, m is also Gaussian and can also be obtained from the surface profile measurements. Alternatively, engineering correlations relating m and σ are available. As given in Bahrami et al.'s review [8], the Lambert and Fletcher correlation represents the data most accurately. The correlation is given by $m = 0.076\sigma^{0.52}$ with σ taken in μm. With both surfaces Gaussian rough, the contact is represented with equivalent surface roughness $\sigma_s = \sqrt{\sigma_1^2 + \sigma_2^2}$ and equivalent asperity slope $m_s = \sqrt{m_1^2 + m_2^2}$.

As the contacting surfaces touch only at the microscopic asperities the area of physical contact, A_p is much smaller than the area of apparent contact, A_a. The surface asperities deform under the applied pressure, p_{app} such that the total applied force is balanced by A_p times the deformation stress at the asperities. The stress dictates whether the deformation is elastic or plastic, which is differentiated by a plasticity index that depends on m, the surface microhardness H_c(taken as that of the softer material), and the equivalent modulus of elasticity, E'. The plasticity index as defined by Tabor [19] is given by $\psi = (E'/H_c)m$, where $E' = 2[(1-\nu_1^2)/E_1 + (1-\nu_2^2)/E_2]^{-1}$; E and ν respectively are the elastic modulus and Poisson's ratio. Plastic deformation occurs when the plasticity index approaches the value of 1 while the deformation is elastic at values much smaller than 1. The following relations hold for A_p [19]:

$$\frac{A_p}{A_a} = \frac{p_{app}}{H_c} \text{(plastic contact)} \tag{2a}$$

$$\frac{A_p}{A_a} = \frac{p_{app}\sqrt{2}}{E'm} \text{(elastic contact)} \tag{2b}$$

Greenwood (in [19]) showed that freshly made surfaces will have a plastic contact even at lightest loads.

During measurements, thermal contact resistance is often observed to depend on the applied force and not the apparent contact area. This is because thermal contact resistance is dictated by the area of physical contact (the area available for heat transfer), which according to Eqs. (2), is proportional to the applied force, $p_{app}A_a$.

The complete derivation of contact resistance models is too rigorous to be included here and only a few model expressions are presented. These models are derived by unifying the thermal analysis, contact mechanics, and deformation analysis summarized above. For the plastic deformation regime, the models are of the form:

$$R_{BC} = \frac{1}{A}\left(\frac{\sigma_s}{m_s}\right)\frac{1}{k_s}\left(\frac{p_{app}}{H_c}\right)^{-B} \tag{3}$$

where the numerical constants, A and B for a few models are listed in Table 1. Despite subtle difference in the assumptions going into the model derivation, which produce slightly different values of A and B, the models yield practically similar values of contact resistance. As an example, Fig. 3 displays the calculated thermal contact resistance for copper-copper joints as a function of applied pressure using the models in Table 1. The calculation uses the following properties: k_s = 285 W/m K, σ_s = 1.6 μm, m_s = 0.09, H_c = 1.3 GPa [20], and A_a = 1 cm^2. In the range of p_{app}/H_c where the models in Table 1 are known to work, the Mikic Rohsenow model predicts 30% higher resistance while the remaining models yield data within 10%. Furthermore, the Yovanovich model has been found to correlate closely to many of the experimental data [8].

2.2. Thermal boundary resistance

On incidence with the physical boundary, the heat carriers will either reflect or transmit on to the other side of the interface. The probability of transmission is less than unity, meaning that for a given temperature difference the actual heat transfer rate is less than if complete transmission was to occur. This translates into an additional resistance to the heat flow across the interface, called the thermal boundary resistance. Extensive work has been reported on thermal boundary resistance for dielectric-dielectric and metal-dielectric contacts where phonons (lattice vibrations) are the heat carriers. We briefly introduce this topic below and direct the readers to [14,15] for in-depth theory, experiments, and review.

Depending upon the surface roughness and the dominant phonon wavelength, the phonons are assumed to transmit either in a specular or a diffuse manner. Early work by Little [14] considered the first case and produced the acoustic mismatch model (AMM) of interfacial thermal resistance. This prevails at extremely low temperatures, typically below 1 K where the dominant phonon wavelength is large (several mm) compared to surface roughness of practical finishes (several micrometers). At higher temperature, the phonon wavelength may become comparable to the surface roughness and in this case, Swartz and Pohl [15] hypothesized that the interface would diffusively transmit the phonons, proposing a phonon diffuse mismatch model (DMM). Dhuley et al. [26] recently explored the phonon DMM in the context of thermal resistance between high purity aluminum and niobium around 4 K. While aluminum is a metal, niobium is a superconductor at this temperature with significant phonon dressing and hence the interfacial heat flow was expected to be due to phonons. The experiments closely followed the temperature dependence predicted by Swartz's DMM and agreed quantitatively to within an order of magnitude.

Based on the DMM methodology for phonons, Gundrum et al. [18] argued that an interface between two metals may transmit electrons diffusively. Their electron DMM is derived here since only the final expression is provided in their paper.

The governing equation for the heat flux crossing an interface from side 1 at temperature T_1 to side 2 at temperature T_2 is:

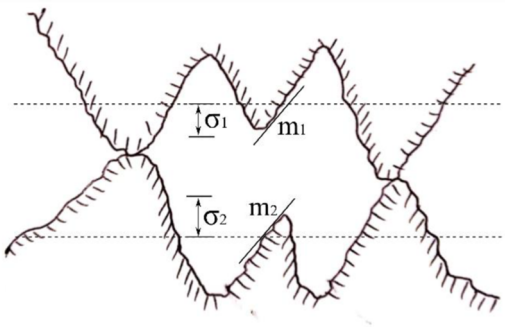

Fig. 2. Contact of two rough surfaces at the microscopic level, displaying the surface roughness, σ and slope is asperity, m on each surface.

Table 1
Parameters of the thermal contact resistance models for plastic deformation regime.

Model	A	B	Validity [5]
Cooper, Mikic, Yovanovich [21]	1.45	0.985	$3.6 \times 10^{-4} < p_{app}/H_c < 1.0 \times 10^{-2}$
Yovanovich [22]	1.25	0.95	$10^{-6} < p_{app}/H_c < 2.3 \times 10^{-2}$
Tien [23]	0.55	0.85	–
Wheeler (from Mikic [24])	1.13	0.94	–
Mikic and Rohsenow [25]	0.9	0.941	–

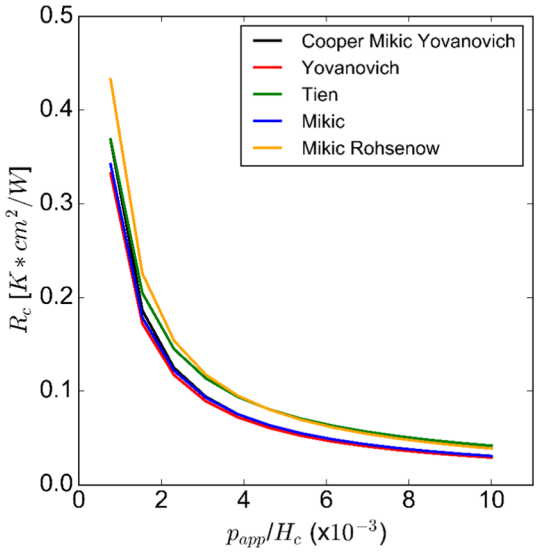

Fig. 3. Thermal contact resistance calculated using the models listed in Table 1. The calculations are for copper-copper pressed contacts with: $k_s = 285$ W/m K, $\sigma_s = 1.6$ μm, $m_s = 0.09$, $H_c = 1.3$ GPa [20], and $A_a = 1$ cm^2.

$$q_{1\to2}(T_1) = \frac{1}{2}\int_0^{\pi/2}\int_0^{\infty} v_1(E)N_1(E,\ T_1)\alpha_{1\to2}(E,\ \theta)(E-\mu)\cos\theta\sin\theta d\theta dE \tag{4}$$

where v and E are the electron speed and energy, $\alpha_{1\to2}$ is the probability of transmission from side 1 to 2, μ is chemical potential, θ is angle of incidence, and N_1 is the density of conduction electrons on side 1, *i.e.*, the product of density of states and the Fermi-Dirac distribution function. A similar equation holds for the flux crossing the interface from side 2 at temperature T_2 to side 1.

The definition of diffuse transmission uses the following two assumptions:

(a) The transmission probability is independent of θ, *i.e.*, $\alpha(E,\ \theta) = \alpha(E)$
(b) The transmission probability from side 1 to side 2 is equal to the reflection probability on side 2, *i.e.*, $\alpha_{1\to2}(E) = r_2(E) = 1 - \alpha_{2\to1}(E)$.

If the two sides are in thermal equilibrium at temperature T, then the net heat flow is zero, *i.e.*, $q_{1\to2}(T) = q_{2\to1}(T)$. Incorporating the assumptions (a) and (b) at thermal equilibrium and if chemical potentials are similar, we have:

$$\begin{aligned} v_1(E)N_1(E,\ T)\alpha_{1\to2}(E) &= v_2(E)N_2(E,\ T)\alpha_{2\to1}(E) \\ &= v_2(E)N_2(E,\ T)(1-\alpha_{1\to2}(E)) \end{aligned} \tag{5}$$

Eq. (5) is known as the principle of detailed balanced [15]. At thermal equilibrium $T = T_2$, $q_{1\to2}(T_2) = q_{2\to1}(T_2)$. In the presence of a temperature difference with the two sides at T_1 and T_2, the thermal boundary resistance is:

$$\begin{aligned} R_{BD}^{-1}(T_1,\ T_2) &= \frac{q_{1\to2}(T_1) - q_{2\to1}(T_2)}{T_1 - T_2} \\ &= \frac{q_{1\to2}(T_1) - q_{1\to2}(T_2)}{T_1 - T_2} \end{aligned} \tag{6}$$

Thus, evaluation of $R_{BD}(T_1,\ T_2)$ requires knowledge of N, v, and α only on side 1 of the interface and the parameters on side 2 are not needed. Inserting Eq. (4) in Eq. (6) and using the incident angle independence of α:

$$\begin{aligned} &R_{BD}^{-1}(T_1,\ T_2) \\ &= \frac{1}{4(T_1 - T_2)}\int_0^{\infty} v_1(E)(E-\mu)[N_1(E,\ T_1) - N_1(E,\ T_2)]\alpha_{1\to2}(E)dE \end{aligned} \tag{7}$$

which for small $T_1 - T_2$ becomes:

$$R_{BD}^{-1}(T) = \frac{1}{4}\int_0^{\infty} v_1(E)(E-\mu)\frac{dN_1(E,\ T)}{dT}\alpha_{1\to2}(E)dE \tag{8}$$

The electron velocity and transmission coefficient are taken to be those of conduction electrons near Fermi level, giving:

$$R_{BD}^{-1}(T) = \frac{1}{4}v_1(E_{F1})\alpha_{1\to2}(E_{F1})\int_0^{\infty}(E-\mu)\frac{dN_1(E,\ T)}{dT}dE \tag{9}$$

The integral is the electronic heat capacity of the solid on side 1. Thus,

$$R_{BD}^{-1}(T) = \frac{1}{4}v_1(E_{F1})\alpha_{1\to2}(E_{F1})C_{v1}(T) \tag{10}$$

Rearranging Eq. (5) gives the expression for the transmission probability:

$$\alpha_{1\to2}(E) = \frac{v_2(E)N_2(E,\ T_1)}{v_1(E)N_1(E,\ T_1) + v_2(E)N_2(E,\ T_2)} \tag{11}$$

which at Fermi level yields:

$$\alpha_{1\to2}(E_{F1}) = \frac{v_{F2}C_{v2}(T)}{v_{F1}C_{v1}(T) + v_{F2}C_{v2}(T)} \tag{12}$$

After substituting Eq. (12) into Eq. (10), and denoting the product vC_v by Z, we have:

$$R_{BD}^{-1}(T) = \frac{Z_1Z_2}{4(Z_1 + Z_2)} \tag{13}$$

For an interface with same material on the two sides, $\alpha_{1\to2} = 0.5$ and

$$R_{BD}(T) = \frac{8}{v_F C_v(T)} \tag{14}$$

A similar expression for phonons was derived by Prasher and Phelan [16] in the ballistic regime ($a \ll$ mean free path). The authors assumed $\alpha_{1\to2} = 1$ and obtained a constant 4 instead of 8 in the numerator of their model expression. This assumption meant that the physical interface by itself did not affect the carrier transport. The expression is similar to the Knudsen flow of a gas through an orifice that is small compared to the gas mean free path.

On substituting the expression of electronic heat capacity C_v (page 144 of [27]), Eq. (14) gives:

$$R_{BD}(T) = \frac{16E_F}{\pi^2 k_B^2 n_e v_F}T^{-1} \tag{15}$$

where n_e is the density of conduction electrons and k_B is the Boltzmann constant. The thermal boundary resistance in Eq. (15) assumes a perfect interface with real contact area equal to the apparent contact area. This condition may hold for interfaces prepared by sputtering, casting, soldering, or welding. For mechanically pressed contacts the physical contact area is smaller than the area of apparent contact and a correction must be made. Using the relation between A_p and A_a(equation (2)), the thermal boundary resistance for a pressed contact becomes:

$$R_{BD}(T) = \frac{16E_F}{\pi^2 k_B^2 n_e v_F} T^{-1} \left(\frac{p_{app}}{H_c}\right)^{-1} \tag{16}$$

expressed per unit apparent contact area.

2.3. Total thermal resistance

The total resistance to heat flow is due to the constrictions and the physical interface between contacting surfaces. Thus, adding Eqs. (3) and (16) in series, the total thermal contact resistance for a joint made of the same material is:

$$R_{BC}(T) = \frac{1}{A}\left(\frac{\sigma_s}{m_s}\right)\frac{1}{k_s}\left(\frac{p_{app}}{H_c}\right)^{-B} + \frac{16E_F}{\pi^2 k_B^2 n_e v_F} T^{-1}\left(\frac{p_{app}}{H_c}\right)^{-1} \tag{17}$$

expressed in terms of the apparent contact area.

2.4. Applicability for low temperature metal-metal contacts

Conduction electrons dominate the thermal properties of metals at cryogenic temperatures. The diffusion limited thermal conductivity, k_s in this case grows linearly with temperature and hence the first term on the right-hand side of Eq. (17) will have T^{-1} dependence. The second right-hand side term is $\sim T^{-1}$ already. Hence, $R_{BC}(T) \sim T^{-1}$. Such behavior is often seen during metallic contact resistance measurements at low temperatures, signifying at least the qualitative applicability of this model. In the final section of this paper, we have made an extensive quantitative comparison of the model predictions and several data from the literature.

Another check to be made is while unifying of the constriction related and interface related components of the thermal contact resistance. For this, we compare the electron mean free path to the average radius of constriction. Assuming all the microscopic asperities are of the same average size and the asperities are plastically deformed, Antonetti and Yovanovich [28] approximated the average spot radius as:

$$a_{avg} = 0.77\left(\frac{\sigma}{m}\right)\left(\frac{p_{app}}{H_c}\right)^{0.097} \tag{18}$$

The electron mean free path is given by:

$$l_e(T) = \frac{3k(T)}{C_v(T)v_F} \tag{19}$$

Consider a copper-copper joint made of OFHC copper with residual resistivity ratio (RRR) of 100. At a temperature of 4.2 K, this copper has $k = 630$ W/m K [29], $C_v = 400$ J/m^3 K, and $v_F = 1.57 \times 10^6$ m/s (page 139 of [27]), which gives $l_e = 3.3$ μm. With $H_c = 1.3$ GPa [20], $p_{app} = 7$ MPa (700 N applied on 1 cm^2 area), and $\sigma = 0.1$ μm (a polished surface), we have $a_{avg} = 2.8$ μm. In this case $a_{avg} \sim l_e$ and both the constriction and thermal boundary resistance are expected to be comparable. As explained by Prasher and Phelan [16], the exact solution of the mixed regime ($a_{avg} \sim l_e$) requires rigorous solution of Boltzmann transport equations and a simpler alternative is to add the two components. Prasher and Phelan [16] in fact have found this solution to closely follow Wexler's solution [17] of the Boltzmann transport equations. Although the surface parameters chosen above are arbitrary, they represent engineering surfaces prepared by common surface machining/polishing processes.

3. Survey of experimental data

3.1. Temperature dependence

The temperature dependence of contact resistance of metallic joints depends on the surface condition and wavelength of the electrons [30]. At low temperatures, the DeBroglie wavelength of conduction electrons in copper is nearly 0.5 nm. If the metallic surfaces are clean of surface oxides, the contact resistance follows T^{-1} dependence similar to the bulk thermal resistance. In case the oxide layer is thick enough not to allow passage of electrons but thin enough to be transparent to phonons, the contact resistance will be governed by the phonon thermal conductivity of the metal. With phonon-electron mean free path $\sim T^{-1}$ and phonon specific heat $\sim T^{-3}$, the phonon thermal resistance varies as T^{-2}. With phonon wavelength of a ~10 nm in copper near 4 K, which is larger than the native oxide thickness of copper of few tens of angstroms, the contact resistance would then go as T^{-2}. In several experiments, the contact resistance across copper-copper pressed contacts is seen to follow a power law T^{-n} where $1 < n < 2$ depending on surface cleanliness. However, a slight exposure to atmosphere is likely to build the native oxide layer on copper and hence the temperature dependence in practical situations is expected to be n close to 2. Finally, when the oxide thickness is much greater than the phonon wavelength in the metal, the contact resistance is controlled by bulk thermal conductivity of the oxide itself.

3.2. Data and experiments

Table 2 presents a summary of our literature survey on thermal resistance of pressed copper contacts. The summary includes joint details (geometry, dimensions, applied force), surface preparation (bare copper, gold-plated copper, surface roughness), temperature range of measurements, thermal conductance observed at 4.2 K, and temperature dependence in the measured temperature range. Special remarks are given in the rightmost column.

Early measurements by Berman [31] and by Berman and Mate [32] investigated thermal resistance between two rods of copper pressed on their ends. With the end application being a heat switch for liquid helium applications, their apparatus allowed making and breaking a cold joint as well as changing the applied force without warming up to room temperature. Although the surface preparation is not specified, the deviation from linear temperature dependence is indicative of a copper-oxide layer on the contacting surfaces. The contact resistance is also somewhat large compared to the other data listed in Table 2. Suomi et al. [33] measured three different joint configurations for use below 0.2 K. Two of these had male-threaded copper that screwed into a female-threaded copper plate. Suomi et al. put forth that the friction while screwing-in the parts cleaned the threads and resulted into a metal-metal contact. The resulting contact resistance was too small to be measured irrespective of the starting conditions of the threads-clean, oxidized, tarnished. A torque no more than finger tightening was necessary. The third joint configuration involved a copper screw whose head pressed against a copper plate while the threads engaged with a threaded epoxy plate on the other side of the copper plate. The differential contraction between the copper and epoxy relaxed the applied force and produced contact resistance larger than in the other two configurations. Nonetheless, the third joint showed linear dependence with temperature.

In a series of measurements with a wide range of applied force, Salerno et al. [34] measured thermal contacts of copper rods pressed on their ends. The joints were made after cooling to 4 K. The contact resistance reported in Table 2 is for the highest applied force of 670 N. Although the samples were surface cleaned, Salerno et al.'s data follow Berman's data in both the temperature dependence (T^{-2}) and value of the resistance.

Nilles [35] measured contacts between the faces of hollow OFHC copper cylinders from 4.2 K to room temperature. In one experiment, they assembled a freshly surface-cleaned joint in a nitrogen gas environment while in another, exposure to air was limited to a few minutes. Due to the limited exposure of these copper samples to air, which kept surface oxidation only to its native nature, the thermal resistance varied near-linearly with temperature. The power law index deviated more from −1 for the sample that was assembled in air. This

Table 2
Survey of thermal contact resistance measurements.

#	Reference	Joint details	Surface details	Temperature range [K]	Thermal contact resistance at 4.2 K [K/W]	Power law	Remark
1	Berman [31]	Pressed rods on ends, surface ϕ1 cm, force 712 N (160 lbf)	bare Cu-Cu, machine finished	2–4.2	80	T^{-2}	
2	Berman and Mate [32]	Pressed rods on ends, surface ϕ1 cm, force 422 N (95 lbf)	bare Cu-Cu	1.5–20	100	$T^{-1.3}$	
3	Suomi et al. [33]	tapered thread, finger tight	bare Cu-Cu, various finishes	0.02–0.2	–	T^{-1}	$4 * T^{-1}$ K/W in 0.02–0.2 K
		flat joint, straight thread, finger tight	bare Cu-Cu, various finishes		–		
		flat joint, straight thread, screwed to an epoxy plate	bare Cu-Cu		–		$36 * T^{-1}$ K/W in 0.02–0.2 K
4	Boughton et al. [44]	concentric cylinders squeezed radially in by a nylon ring, surface ϕ0.46 cm × 0.8 cm	gold plated Cu-Cu	1.2–4.2	12.8	$aT^{-1} + bT^{-2}$	a = 153.85 K/W, b = 344.8 K^2/W, electrical resistance also measured
5	Salerno et al. [34]	pressed rods on ends, surface ϕ10.2 mm, force 670 N	bare Cu-Cu, 0.4 μm roughness	1.6–4.8	100	T^{-2}	joint made after cooling; several lower forces also measured
6	Van Sciver et al. [13]	pressed hollow cylinders on ends, surface 0.1 cm^2, pressure 7 MPa	bare Cu-Cu, 0.1 μm roughness	5–25	1.8	T^{-1}	surface reported as machined
7	Nilles [35]	pressed hollow cylinders on ends, surface 0.1 cm^2, force 137 N	bare Cu-Cu, 0.1 μm roughness	4.2–12	5.6	$T^{-1.2}$	assembly in nitrogen gas enclosure, thermal resistance also measured
				4.2–12	8.4	$T^{-1.4}$	assembly in air, thermal resistance also measured
8	Kerr and Horner [37]	pressed plates, surface 0.5 × 0.5 in^2, torque 25 in-lbf on an 8–32 SS nut-bolt	bare Cu-Cu, clean	3.6–5.6	0.6	–	
			bare Cu-Cu, tarnished	3.4–5.2	0.9		
			gold plated Cu-Cu	3.2–4.6	0.08		
9	Kittel et al. [39]	pressed rods on ends, surface ϕ10.2 mm, force 670 N	gold plated Cu-Cu, 0.8 μm lapped finish before plating	1.8–6	65	$T^{-2.15}$	joint made after cooling; several lower forces also measured
10	Sunada and Kang [36]	pressed hollow cylinders on ends, surface 1.4 cm^2, 20 MPa pressure	bare Cu-Cu		0.06		
11	Didschuns et al. [42]	flat joint	gold plated Cu-Cu	0.33–0.42		T^{-1}	
		- surface 87 mm^2, torque 125 N cm, one M4 screw			–		16.7 K/W projected at 1 K, damaged due to excessive torque
		- surface 68 mm^2, torque 65 N cm, two M2 screws			–		10 K/W projected at 1 K
		- surface 159 mm^2, torque 100 N cm, two M3 screws cylindrical clamp			–		5.9 K/W projected at 1 K
		- surface 94 mm^2, torque 150 N cm, one M2 screw			–		6.5 K/W projected at 1 K
		- surface 94 mm^2, torque 65 N cm, two M2 screws			–		15 K/W projected at 1 K
		- surface 132 mm^2, torque 76 N cm, four 4–40 screws			–		11 K/W projected at 1 K
12	Bintley et al. [38]	concentric hollow copper cylinders on a central core of Invar (compression joint), surface 745 mm^2	bare Cu-Cu	0.1–1	–		100 K/W at 1 K, 10 K/mW at 0.1 K
			gold plated Cu-Cu	0.1–0.25, 6–7	–	T^{-1}	100 K/W at 0.1 K, 10 K/W at 6 K
13	Schmitt et al. [40]	flat joint					
		- surface 0.75 in × 0.75 in, torque 25 in-lbf, 10–32 SS screw	citric acid passivated bare Cu-Cu, 0.2 μm	0.3–1, 6–18	–	$T^{-1.43}$	$27 * T^{-1.43}$ fits all data
		- surface 0.75 in × 0.75 in, torque 25 in-lbf, 10–32 SS screw	gold plated Cu-Cu, 0.2 μm before plating	0.1–0.5, 4–10	1.7	$T^{-1.11}$	$8.6 * T^{-1.11}$ fits all data
		- surface 1 in × 0.75 in, torque 25 in-lbf, 10–32 SS screw	gold plated Cu-Cu, 0.4 μm before plating	0.06–0.15, 6–26	–		

(*continued on next page*)

Table 2 (*continued*)

#	Reference	Joint details	Surface details	Temperature range [K]	Thermal contact resistance at 4.2 K [K/W]	Power law	Remark
14	Dillon et al. [41]	flat joint, surface 2.32 cm^2		3–20			
		- Force 458.4 N	bare Cu-Cu, 1.6 μm roughness		33		
		- Force 62.3 N			143		
		- Force 458.4 N	gold plated Cu-Cu, 1.6 μm		1.7		
		- Force 62.3 N	roughness before plating		5		
		- Force 62.3 N	gold plated Cu-Cu, 0.1 μm roughness before plating		3.3		
15	Dhuley et al. [43]	cylindrical clamp					
		- surface 4.5 cm^2, force 4.5 kN	gold plated Cu-Cu, 0.4 μm	0.23–7.5	0.44	$T^{-1.19}$	$2.4 * T^{-1.19}$ fits all data
		- surface 28.7 cm^2, force 4.5 kN	roughness before plating	2.9–8.3	0.23	$T^{-1.13}$	$1.16 * T^{-1.13}$ fits all data

study shows that any practical copper joint assembly procedure involving exposure to air will produce a surface oxide layer, which will increase the thermal contact resistance. Nonetheless, their joints had an order of magnitude lower thermal contact resistance than Berman [31] and Salerno et al. [34]. Nilles also purposefully grew thicker (1000 Å) copper oxide and found that these joints show T^{-2} variation. Furthermore, Nilles measured electrical contact resistance on their joints. The observations are discussed along with other electrical contact resistance data in a subsequent section.

Sunada and Kang [36] measured end-to-end copper cylinders pressed with a large force (2.8 kN) and obtained 0.06 K/W at 4.2 K, which is the lowest value of thermal contact resistance found during the present survey. Neither the temperature dependence nor the joint/surface cleaning methodology is reported in their paper.

Due to its low oxygen affinity, gold plating of copper is an effective approach of preventing surface oxides and achieving electronic thermal conductance across pressed contacts. Additionally, native surface oxide of gold breaks at low applied load thereby giving a larger probability of achieving a metallic contact [32]. Another advantage of gold is its lower surface hardness than copper. Consequently, gold plated contacts have larger area of physical contact (see equation (2)) and therefore lower thermal resistance for a given applied force.

Several researchers have studied gold-plated copper-copper contacts for use below 4.2 K and especially at sub-Kelvin temperatures. Comparative studies of bare copper-copper and gold-plated copper-copper contacts by Kerr and Horner [37], Bintley et al. [38], Salerno et al. [34] and Kittel et al. [39], Schmitt et al. [40], and Dillon et al. [41] have shown that gold plating can lower the resistance by as much as an order of magnitude around 4.2 K and below. At sub-Kelvin temperatures, measurements of gold-plated contacts have been typically made to qualify specific joint configurations for specific end-applications. Detailed parametric studies are rare. The commonly used joint configurations are flat plates bolted together as by Didschuns et al. [42] and Schmitt et al. [40], bolted circular clamps around a circular rod as by Didschuns et al. [42] and Dhuley et al. [43], and concentric cylindrical joints pressed radially by differential thermal compression. For the latter, Boughton et al. [44] used a nylon ring outside of a pair of concentric cylinders while Bintley et al. [38] placed a pair of concentric cylinders around an invar core. On cooling to base temperature, excess compression of nylon produced the pressing radial force in the case of Boughton. On the other hand, the copper pair shrunk radially inward more than invar, thereby generating the pressing force in Bintley et al.'s configuration. Both Boughton et al. and Bintley et al. caution that careful machining tolerances are needed to achieve good compression-type joints.

The thermal resistance data presented in Table 2 for gold-plated copper-copper contacts vary as T^{-1} with temperature, which is a signature of clean metal-metal contacts. The thermal transport over these contacts is electronic and so an accurate physical basis exists for extrapolating such data to lower temperatures.

Direct measurement of thermal contact resistance at cryogenic temperatures requires proper selection of instrumentation (thermometers, heaters, lead wires), accurate determination of heat fluxes (including stray heat leaks) and temperatures, and often a complicated uncertainty analysis [35]. The measurements become more complex (and expensive) as the temperature is lowered below 4.2 K. A simpler alternative, which researchers have relied on for metal-metal contacts, is to measure electrical resistance and convert this to thermal resistance using the Wiedemann-Franz law (page 156 of [27]):

$$R_{BCt} = \frac{R_{BCe}}{L_0} T^{-1} \tag{20}$$

Here R_{BCt} and R_{BCe} respectively denote thermal and electrical resistance, and L_0 is a constant called the Lorenz number, which in theory is material independent. With R_{BCe} being independent of temperature around 4.2 K and below, R_{BCt} for < 4.2 K can be estimated based on

Table 3
Survey of electrical contact resistance measurements at 4.2 K.

#	Reference	Joint details	Surface details	Resistance [μΩ]	Remarks
1	Boughton et al. [44]	Concentric cylinders squeezed radially in by a nylon ring			
		- surface ϕ1.83 cm × 2.2 cm	Bare Cu-Cu	28	
			Gold plated Cu-Cu	0.3	
		- surface ϕ0.34 cm × 0.6 cm		11	
		- surface ϕ0.46 cm × 0.8 cm		9.5	Thermal resistance also measured
2	Meuthing et al. [48]	CONCENTRIC cylinders squeezed radially in by a nylon ring, surface ϕ1.98 cm × 3.81 cm	Gold plated Cu-Cu	0.041	
		Tapered 1/8 NPT thread		1.3	
		Pressed plates, surface 2 cm^2, 4–40 SS screw		0.4	
3	Manninen and Zimmerman [49]	Pressed plates, surface 7 mm × 4 mm, 4 mm SS screw, torque 0.8 N m	Bare Cu-Cu, sanded with 600 grit emery paper	0.2	
4	Lau and Zimmerman [50]	Pressed hollow cylinders on ends, surface 30 mm^2, 8–32 screw (SS, Cu, Brass), torques 0.8 Nm, 1.6 N m	Bare Cu-Cu, sanded with 600 grit emery paper	0.13	
		pressed hollow cylinders on ends, surface 30 mm^2, 8–32 screw (SS, Cu, Brass), torque 1.6 N m	Gold plated Cu-Cu	0.04	
5	Deutsch [51]	Pressed plates, surface 10 mm × 10 mm, 8–32 SS screw bare Cu-Cu, sanded with 600 grit emery paper screw, torque 4 N m	Bare Cu-Cu, sanded with 600 gr bare Cu-Cu, sanded with 600 grit emery paper	0.2	
6	Okamoto et al. [46]	Pressed discs on ends, surface ϕ9 mm, 4 mm screw			
		- Torque 4 N m	Bare Cu-Cu, sanded with 100 grit emery paper	0.0299	
			Bare Cu-Cu, sanded with 400 grit emery paper	0.015	
			Bare Cu-Cu, polished with 3000 grit emery paper	0.034	
			Gold plated Cu-Cu	0.01	
		- Torque 5 N m	Gold plated Cu-Cu, polished with 3000 grit emery paper before plating	0.0087	
7	Noterdaeme [47]	Pressed discs on ends, surface 1.4 cm^2, bare Cu-Cu pressure 170 MPa	Bare Cu-Cu	0.0045	
			Silver plated Cu-Cu	0.0005	
8	Nilles [35]	Pressed hollow cylinders on ends, surface 0.1 cm^2, force 137 N	Bare Cu-Cu, 0.1 μm roughness	0.41	assembly in nitrogen gas enclosure, thermal resistance also measured
				1.19	assembly in air, thermal resistance also measured
9	Blondell et al. [45]	Pressed plates, surface 1 cm × 1 cm, force 3000 N applied using M4 SS screw	Bare Cu-Cu (as received)	0.23	
			Bare Cu-Cu, sanded with 400 grit emery paper	0.14	

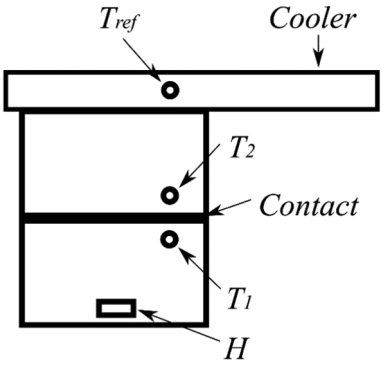

Fig. 4. Steady heat flow method for thermal contact resistance measurement, implemented on a 4 K cryocooler. H = heater, T = thermometer.

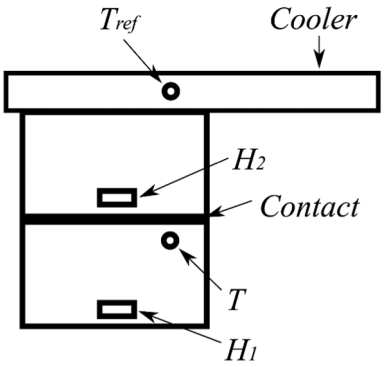

Fig. 5. The two-heater method for contact resistance measurement as implemented on a cryocooler. H = heater, T = thermometer.

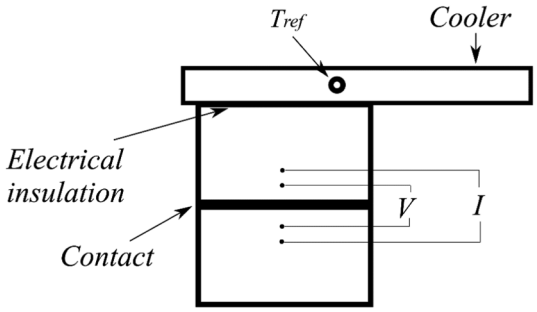

Fig. 6. Apparatus for the DC four wire method of contact electrical resistance measurement.

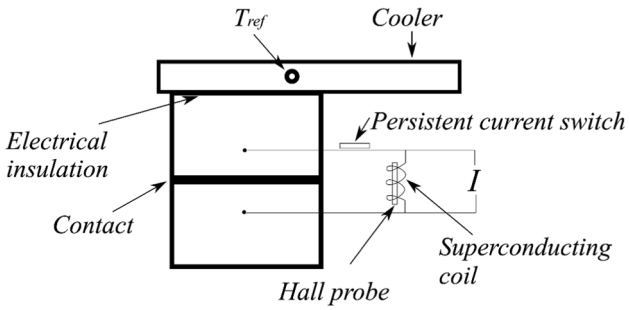

Fig. 7. Apparatus for contact electrical resistance method *via* a decay time measurement [46].

the 4.2 K measurement of R_{BCe}.

Table 3 presents our survey of electrical contact resistance measurements at 4.2 K for both bare copper-copper and gold-plated copper-copper contacts. Different joint configuration- pressed flat plates, compression-pressed concentric cylinders, and bolted plates have been tested by researchers. We note the following:

(a) Gold-plated copper-copper joints can yield < 10 nΩ and are less resistive than bare copper-copper joints (typically tenths of a μΩ)
(b) Electrical contact resistance of bare copper-copper joints is sensitive to surface preparation- clean contacts produce significantly lower resistance [35,45,46].
(c) Among the surveyed data, Noterdaeme [47] has reported the lowest electrical contact resistance of 0.5 nΩ across a silver-plated copper-copper contact. The contact carried a high pressure of 170 MPa. However, silver is more prone to surface oxidation than gold when exposed to air [47].

The Wiedemann-Franz law concerns with only the electronic transport in metals. Because an additional transport by phonons may be present across the contact the effective thermal resistance will be lower than that given by the Wiedemann-Franz law. The electrical contact resistance measurement approach therefore gives an upper bound of thermal contact resistance. The simultaneous measurements of thermal and electrical contact resistance by Nilles [35] and by Boughton et al. [44] noted the experimental values of Lorenz number to be greater than the theoretical, indicative of heat transfer channels in addition to electronic.

4. Measurement techniques

In this section, we will look at some of the experimental techniques for the measurement of contact resistance. All these techniques can be implemented on a closed-cycle 4 K cryocooler, which typically has cooldown-warmup cycle of a few hours, thereby facilitating quick turnaround of the measurement routine.

The common technique for direct thermal contact resistance measurement is the steady heat flow method. As depicted in Fig. 4, a thermal contact to be measured is connected to the cryocooler base plate. Thermometers, T_1 and T_2 are placed across the contact while a heater, H placed on the far side of the contact generates the required heat flow. At a steady state, which can be noted from the reference thermometer, T_{ref} the contact resistance is determined as $(T_1 - T_2)/Q$, where Q is the heat flow. This value of the contact resistance corresponds to the average temperature of $0.5(T_1 + T_2)$ and care should be taken to ensure that $(T_1 - T_2)$ is small compared to the average temperature. Typically suggested values of $(T_1 - T_2)$ is 1–2% of T_{ref} [35]. As an example, if a contact resistance measurement is to be carried out at 4 K, $(T_1 - T_2) \approx$ 40–80 mK. If one uses Cernox thermometers with typical accuracy of 5 mK near 4.2 K [52], the measurement introduces 8–10 mK error in the temperature difference. Therefore, in this scenario, the contact resistance inherently carries at least 10–20% uncertainty. Attention should also be paid while locating T_1 and T_2 as they should be as close to the contact as practical, otherwise bulk resistance of the block appear in the measurement. The bulk resistance can be subtracted if the bulk material conductivity is known or by installing a linear array of thermometers along the heat flow path on each side of the contact. The latter arrangement will yield both the material bulk resistance and the contact resistance but will also need more tedious uncertainty analysis stemming from the accuracy of each thermometer. The technique will also be expensive as it requires a greater number of accurate thermometers. Nonetheless, OFHC copper has substantial thermal conductivity around 4 K and hence the contribution of bulk resistance can typically be neglected in the steady heat flow method. Nilles [35] has given implementation details and uncertainty analysis of the stead heat flow technique.

A thermodynamic equivalent of the steady heat flow technique but more relaxed with uncertainty analysis is the two-heater technique as depicted in Fig. 5. The contact to be measured is mounted on the

Table 4
Properties of copper and plating gold used in the model evaluation.

Property	Copper (OFHC)	Gold
Density [kg/m^3]	8960	19,320
Fermi velocity [m/s] (page 139 of [27])	1.57×10^6	1.38×10^6
Fermi energy [eV] (page 139 of [27])	7.00	5.51
Free electron density [1/m^3] (page 139 of [27])	8.47×10^{28}	5.9×10^{28}
Effective electron mass multiplier [–] (page 146 of [27])	1.34	1.14
Bulk thermal conductivity at 4.2 K [W/m K]	4.2 * (1.44 * RRR + 5.23) (derived using data from [29])	140 [53] (plating grade)
Microhardness [GPa]	1.3 [20]	0.69 [54] (plating grade)

Table 5
Directly measured thermal resistance data and model calculation for clean copper-copper and gold-plated copper-copper pressed contacts.

Reference	Contact area [cm^2]	Force [kN] or (pressure [MPa])	T range [K], (observed power law)	Thermal contact resistance at 4.2 K [K cm^2/W]				DMM/ Constriction	Reported/ Model total	Surface roughness [μm]	RRR
				Reported	Constriction model	DMM model	Model total				
Copper-copper contacts (reported as clean)											
Van Sciver et al. [13]		(7)	–, (T^{-1})	1.83	8.4×10^{-3}	0.024	0.032	2.9	57	0.1	112
Salerno et al. [34]	0.812	0.67	1.6–4.2, (T^{-2})	113.4	0.018	0.028	0.046	1.6	2464	0.4	100 (assumed)
Nilles [35]	0.1	0.137	4.2–12, ($T^{-1.2}$)	0.56	4.4×10^{-3}	0.012	0.016	2.7	34	0.1	112
Sunada and Kang [36]	–	(20)	–	0.049	0.013	8.3×10^{-3}	0.021	0.6	2.3	1.6 (assumed)	100 (assumed)
Schmitt et al. [40]	3.61	0.9	0.3–18, ($T^{-1.43}$)	12.52	0.028	0.067	0.095	2.4	132	0.2	100 (assumed)
Dillon et al. [41]	2.32	0.458	3–20, (–)	77.3	0.095	0.084	0.18	0.9	432	1.6	125
		0.063		331.4	0.63	0.62	1.25	1	265		
Gold-plated copper-copper contacts											
Kittel et al. [39]	0.812	0.67	1.6–4.2, ($T^{-2.15}$)	52.6	0.23	0.073	0.33	0.3	176	0.8	–
Didschuns et al. [42]	0.68	0.22	0.33–0.42, (T^{-1})	3.93 (at 1 K)	0.84	0.195	1.04	0.2	3.8	1.6 (given 'as machined')	–
	1.59	0.47		9.35 (at 1 K)	0.417	0.093	0.51	0.2	18.3		–
Schmitt et al. [40]	3.61	0.9	0.1–10, ($T^{-1.11}$)	6.35	0.097	0.06	0.157	0.6	40.4	0.2	–
Dillon et al. [41]	2.32	0.458	3–20, (–)	3.87	0.33	0.076	0.40	0.2	9.6	1.6	–
		0.063		11.6	2.17	0.56	2.73	0.3	4.3	1.6	–
		0.063		7.73	0.57	0.56	1.13	1	6.8	0.1	–

cryocooler plate in the same way as in Fig. 4. This technique, however, uses two heaters, one upstream (H_1) and the other downstream (H_2). Only one thermometer (T) is required and is placed upstream of the contact. The measurement routine is as follows:

(a) Pass a heat current 'Q' into H_1, measure $T = T_a$ at steady state. The heater H_2 is off in this step.
(b) Pass the same heat current 'Q' into H_2 with H_1 off. Measure $T = T_b$ at a steady state.
(c) Calculate the thermal resistance as $(T_a - T_b)/Q$.

The two-heater method uses the fact that as long as Q is equal in steps a and b, T_{ref} will remain unchanged as T_{ref} is purely a function of Q for a given cryocooler. If T_{ref} is unchanged, then the downstream block (on which H_2 is mounted) will be at the same temperature in steps a and b. Because no heat flows across the contact in step b, both the upstream and downstream plates will read the same temperature. It then follows that T_b is equal to the downstream plate temperature in step a as well as in step b. Hence, $T_a - T_b$ is the temperature difference across the contact in step a.

The two-heater technique offers several advantages over the steady heat flow technique. The two-heater technique requires one accurate thermometer as opposed to two, which saves on the cost of thermometers (accurate 4 K thermometers are expensive). Inexpensive metal film resistors can serve as the heaters. As the temperature difference is small (T_a and T_b not very different) and is measured using the same thermometer, the uncertainty that propagates into $T_a - T_b$ will be substantially smaller than in the method that uses two distinct thermometers. The two-heater method however requires the same heat flow through the two heaters. Although this requires care, very similar (within 1%) heat flow can be achieved by choosing matched resistors for H_1 and H_2 and adjusting the current flow into the heater such that T_{ref} between steps a and b is unchanged. As T_{ref} is purely a function of the heat flow into the cryocooler, an unchanged T_{ref} will mean that the same amount of heat is flowing through H_1 and H_2 in steps a and b respectively. As with the steady heat flow method, the two-heater method also requires carefully placement of the thermometer, as close to the contact as practical. This method was used by Bintley et al. [38], Schmitt et al. [40], Didschuns et al. [42], and Dhuley et al. [43] for sub-Kelvin thermal contact resistance measurements.

An indirect method of determining thermal contact resistance is to measure electrical resistance of the contact and convert into thermal

Table 6
Measured electrical resistance data at 4.2 K converted to thermal resistance using Wiedeman-Franz law, assuming the theoretical value of Lorenz number, 2.45×10^{-8} WΩ/K^2. The equivalent thermal resistance is compared to model predictions.

Reference	Contact area [cm^2]	Force [kN] or (pressure [MPa])	Reported electrical contact resistance at 4.2 K [μΩ]	Thermal contact resistance at 4.2 K [K cm^2/W]				DMM/ constriction	WF law prediction/ Model total	Surface roughness [μm]	RRR
				WF law prediction	Constriction model	DMM model	Model total				
Copper-copper contacts (reported as clean)											
Manninen and Zimmerman [49]	0.322	0.15	0.2	0.626	0.075	0.036	0.11	0.5	5.6	0.13	30
Notardaeme [47]	1.43	(170)	0.0045	0.063	1.7×10^{-3}	9.8×10^{-4}	0.003	0.6	23.4	1.6	100 (assumed)
Deutsch [51]	0.864	1.4	0.057	0.478	4.8×10^{-4}	0.01	0.01	20.8	45.6	0.13	1034
Lau and Zimmerman [50]	0.3	0.15	0.13	0.38	7.4×10^{-3}	0.033	0.04	4.4	9.4	0.13	200
Okamoto et al. [46]	1.64	1.4	0.0299	0.48	7.4×10^{-4}	0.02	0.021	27.1	23	1.5	4000
			0.0151	0.24	3×10^{-4}	0.02	0.02	65.4	11.9	0.24	
			0.0344	0.55	2×10^{-4}	0.02	0.02	99.6	27.1	0.1	
Gold-plated copper-copper contacts											
Meuthing et al. [48]	2	1.1	0.4	7.78	0.033	0.027	0.06	0.8	129.6	0.1 (mirror finish)	–
Lau and Zimmerman [50]	0.3	0.3	0.04	0.12	0.021	0.015	0.036	0.7	3.3	0.13	–
Okamoto et al. [46]	1.64	1.4	0.01	0.16	0.022	0.018	0.04	0.8	4	0.1	–
		1.75	0.0087	0.14	0.017	0.014	0.031	0.8	4.5	0.1	–

resistance using the Weideman-Franz law. A measurement apparatus comprising of a current source and a voltmeter (preferable a nanovoltmeter) can be used for such a measurement. The DC four-wire method implemented on a contact attached to a cryocooler is depicted in Fig. 6. In this arrangement, it is imperative to place an electrical insulator with decent thermal conductivity between the cryocooler plate and the joint assembly. The voltage taps should be close to the contact so that the bulk resistance contribution to the measured resistance is small. Moderately high electrical contacts (tenths of a μΩ) can be measured with the DC four-wire method using laboratory instruments such as the Lake Shore Cryotronics 121 current source and Keithley 2182A nanovoltmeter. Assume that the contact resistance is 1 μΩ. The current source can be powered to 100 mA, giving 100 nV on the voltmeter. Referring to the typical accuracies of these instruments, the contact electrical resistance can be measured with about 10% accuracy. If higher accuracy is desired, one may use a current source with higher current output capability, which will also require larger current leads to the plates, resulting into increased heat leak into the sample. The DC four-wire method with the instruments stated above may prove inadequate for measuring resistances of the order of nΩ or lower.

Smaller electrical resistance (nΩ and lesser) can be measured using the electrical current decay method as outlined by Okamoto et al. [46]. As depicted in Fig. 7, a superconducting LR circuit comprising of superconducting lead wires and a solenoid coil is arranged across the contact. The circuit inductance stems from the solenoid while the resistance primarily is due to the pressed contact. The switch on one of the lead wires serves to enable/disable the persistent current mode. Starting with the persistent mode off (lead wire in resistive mode), the input current energizes the coil. Next, the input current is turned off and the persistent mode is turned on (lead wire becomes superconducting) so that the energy stored in the coil decays across the pressed contact resistance. The energy (magnetic flux) decay with time is read by a Hall probe sensor located in the superconducting coil and the contact resistance R_c is obtained by determining the decay time constant L/R_c. Using a lead wire superconducting coil (diameter 6 mm, length 12 mm, 20 turns) with an inductance of 2.75 μH, Okamoto et al. [46] measured electrical contact resistance as small as 4 nΩ with an accuracy of better than 1 nΩ. Their apparatus used a mu-metal magnetic shield around the contact so that ambient magnetic field had a minor contribution to the Hall probe reading. An even more accurate but rigorous current decay technique was developed by Noterdaeme [47] that enabled measuring contact resistance as small as 0.5 nΩ.

5. Model and data comparison for flat contacts

In this section, we evaluate Eq. (17) and compare with the data for flat contacts listed in Tables 2 and 3. We use the Yovanovich correlation parameters from Table 1 for the constriction resistance term and conduction electron parameters to evaluate the boundary resistance term. Table 4 lists values of these parameters for copper and gold. These parameters are taken from [27]. Temperature and purity dependent thermal conductivity of copper is derived from the NIST data [29]. Where RRR of copper is not reported in the source literature, we have taken it as 100. Unlike copper, RRR is gold is not reported and so thermal conductivity of plating-grade gold is taken as 140 W/m K at 4.2 K as noted by Bernat et al. [53]. Surface hardness of copper and gold are likely to vary from sample to sample and none of the surveyed papers have reported the values for their samples. To allow for the model-data comparison, we chose the following values of surface microhardness: copper – 1.3 GPa [20] and gold – 0.78 GPa [54]. Both these values are at room temperature, where most of the contacts are assembled. Notable exceptions include Salerno et al. [34] and Kittel et al. [39] who made the contacts after cooling to 4 K.

Both the constriction and boundary resistance terms in equation (17) require the value of applied pressure. In several cases, the researchers in Tables 2 and 3 have reported either the applied pressure or

the contact area and applied force. In some cases, the screw size, material, and the applied torque are specified. For the latter case, we estimated the force using the bolt torque-tension relation given in [55]. The Appendix A summarizes the bolt tension calculation.

For the cases that have not reported surface roughness of copper, we have assumed the commonly specified roughness of 1.6 μm. Roughness of the gold-plated surface is taken to be equal to the roughness of the copper base. In all cases, the average slope of asperities is calculated using the Lambert-Fletcher correlation [8].

Tables 5 and 6 present a comparison of the calculated thermal conductance (equation (17)) with the experimental data from the literature. Table 5 includes comparison of the directly measured thermal resistance. In Table 6, the measured electrical resistance is converted to thermal resistance using the Wiedemann-Franz law and then compared with the model prediction. We used the theoretical Lorenz number value of 2.45×10^{-8} WΩ/K^2 for converting the electrical resistance to thermal resistance.

The main results included in Tables 4 and 5 are the calculated thermal constriction resistance (Yovanovich correlation), calculated thermal boundary resistance (diffusion mismatch model or DMM), calculated total thermal resistance, ratio of the boundary to constriction resistance, and ratio of the reported experimental to total calculated resistance. We infer the following:

(a) In all the cases, the boundary resistance is at least comparable to the constriction resistance and hence should not be neglected at cryogenic temperatures. For the coppers with RRR ~100, both the components are nearly equal. Constriction resistance dominates at low RRR (Manninen and Zimmerman [49], RRR = 30) while boundary resistance dominates in higher purity copper (Okamoto et al. [46], RRR = 4000; Deutsch [51], RRR = 1034) in the case of bare copper-copper contacts. For the surveyed gold-plated contacts, the boundary resistance is comparable to the constriction resistance. The effect of purity of gold (RRR) is not clear since a single value of 140 W/m*K for gold's thermal conductivity was used in this study.

(b) Gold plated contacts agree reasonably with the model calculations. Out of the total 11 data surveyed, 7 agree to within an order of magnitude, 2 are within a factor of 40, while the largest deviation is 130-fold. Kittel et al.'s [39] data are 176 times larger than the model calculation. The reason for this large deviation is unclear and so the following explanation is offered: their contacts were made at 4 K, where surface microhardness of gold is larger than the room temperature value used in present calculations. Furthermore, Kittel et al.'s data show $T^{-2.15}$ dependence, which indicates that the gold-plated samples may not have a metal-metal contact.

(c) Contacts with ~T^{-1} variation in general show reasonable agreement (well within a factor of 100) with the model. This holds for gold-plated as well as bare copper-copper contacts. The deviation increases as the power law exponent reduces below −1 (see the data of bare copper-copper contacts of Nilles [35], Schmitt et al. [40], and Salerno et al. [34] in order). To conclude, the model predicts well the resistance of contacts that are metallic in nature.

Out of the 25 experimental data surveyed, the model calculations agree with 11 data points with < 10-fold deviation and with another 8 data points with < 100-fold deviation. Excluding the contacts made at 4.2 K (Salerno et al. [34] and Kittel et al. [39]), the maximum deviation is 432-fold for Dillon et al.'s data [41]. Several sources of errors exist in the present model calculations that cannot be quantified- the use of Lambert and Fletcher relation between m and σ, the relation between torque and force exerted by a screw, and neglect of sample to sample variation of surface microhardness of copper and gold. In view of all these sources of errors, we believe that the model shows a fair trend with the thermal resistance data of copper contacts at cryogenic temperatures around 4 K and below.

6. Summary and outlook

This paper summarizes the experimental investigations from the nearly fifty years made on pressed copper contacts for designing demountable joints with high thermal conductance at 4 K and colder. Despite of the utmost care exercised during cleaning and assembly of bare copper joints, these showed a temperature power law T^{-n} with $-2 < n < -1$, indicative of a surface oxide layer. The surveyed gold-plated copper joints were largely metallic (T^{-1}) because gold has lower oxygen affinity and the surface oxide layer breaks on application of pressure during joint assembly.

We briefly reviewed the thermal constriction resistance models and derived a thermal resistance model based on diffuse electron transmission across a metal-metal boundary. The constriction and boundary resistance models are unified using Prasher and Phelan's [16] approach and the resulting model agrees reasonably with a large portion of the surveyed experimental data. The theory-experiment match is prominent among the gold-plated contacts due to their metallic nature.

Despite their advantages over bare copper contacts, no systematic study is so far reported on gold-plated contacts. Experimental measurements are limited to trial and error to the extent of obtaining sufficient thermal conductance for a given end-application. Given that the metallic nature of gold-plated joints can be achieved easily (without special shielding from atmospheric oxygen) and their fair agreement with the theoretical model, we suggest a programmatic experimental study of gold-plated copper contacts. This study should investigate all important parameters that appear in the theoretical model- surface roughness, microhardness, thermal conductivity of plating-grade gold, applied force, and culminate in comparison with the model. The model-experiment agreement, if found promising, can provide a definitive reference for the design of future ultra-low temperature experiments that would otherwise continue to rely on trial and error.

Declaration of Competing Interest

The author declares no conflicts of interest.

Acknowledgements

This manuscript has been authored by Fermi Research Alliance, LLC under Contract No. DE-AC02-07CH11359 with the U.S. Department of Energy, Office of Science, Office of High Energy Physics.

Appendix A

The screw force is estimated from the applied torque, τ_{screw} using the relation given in [55] in SI units:

$$F_{screw} = \frac{\tau_{screw}}{0.16P + 0.58\mu d + 0.25\mu_b(d_s + d_h)} \quad \text{(A1)}$$

In Eq. (A1), P is the thread pitch, μ is thread friction coefficient, d is thread diameter, μ_b is friction coefficient between the screw head and joint surface, d_s is diameter of screw head, and d_h is screw clearance hole diameter. We have used $\mu = \mu_b = 0.53$ for a steel screw in copper threads and 1 for copper screw in copper threads [56]. Table A1 lists the screw parameters for screw sizes appearing in Tables 2 and 3.

Table A1
Screw parameters for screw sizes appearing in Tables 2 and 3.

	All dimensions in mm			
Thread	P	d	d_s	d_h(close fit)
4–40	0.635	2.79	4.64	2.94
8–32	0.794	4.06	6.85	4.30
10–32	0.794	4.82	7.93	4.97
M2	0.4	2	3.8	2.4
M3	0.5	3	5.5	3.4
M4	0.7	4	7	4.5

References

[1] Richards SN, et al. SOFIA-HIRMES: looking forward to the HIgh-Resolution Mid-infrarEd Spectrometer. J Astronom Instrum 2018;7(4):1840015. https://doi.org/10.1142/S2251171718400159.

[2] Hollister MI, Bauer DA, Dhuley RC, Lukens P, Martin LD, Ruschman MK, Schmitt RL, Tatkowski GL. The cryogenics design of the SuperCDMS SNOLAB experiment. IOP Conf SeriesMater Sci Eng 2017;278:012118. https://doi.org/10.1088/1757-899X/278/1/012118.

[3] Durandetto P, Monticone E, Serazio D, Sosso A. Thermal performances of an improved package for Cryocooled Josephson standards. In: IEEE transactions on components, packaging and manufacturing technology (Early Access). (https://doi.org/10.1109/TCPMT.2019.2901297).

[4] Krinner S, Storz S, Kurpiers P, Magnard P, Heinsoo J, Keller R, et al. Engineering cryogenic setups for 100-qubit scale superconducting circuit systems, arXiv:1806.07862; 2018 (https://arxiv.org/abs/1806.07862).

[5] Lambert MA, Fletcher LS. Review of models for thermal contact conductance of metals. J Thermophys Heat Transfer 1991;11(2):129–40. https://doi.org/10.2514/2.6221.

[6] Madhusudana CV, Fletcher LS. Thermal contact conductance: a review of recent literature. Tech. Rep. College Station (TX, USA): Texas A & M University; September 1981.

[7] Sridhar MR, Yovanovich MM. Critical review of elastic and plastic thermal conductance models and comparison with experiment, paper no. 93-2776. In: 28th AIAA Thermophysics conference, Orlando, FL, July 6–9; 1993. (https://doi.org/10.2514/6.1993-2776).

[8] Bahrami M, Culham JR, Yananovich MM, Schneider GE. Review of thermal joint resistance models for nonconforming rough surfaces. Appl Mech Rev 2006;59(1):1–12. https://doi.org/10.1115/1.2110231.

[9] Yovanovich MM. Four decades of research on thermal contact, gap, and joint resistance in microelectronics. IEEE Trans Compon Packag Technol 2005;28(2):182–206. https://doi.org/10.1109/TCAPT.2005.848483.

[10] Gmelin E, Asen-Palmer M, Reuther M, Villar R. Thermal boundary resistance of mechanical contacts between solids at sub-ambient temperatures. J Phys D Appl Phys 1999;32:R19–43. https://doi.org/10.1088/0022-3727/32/6/004.

[11] Woodcraft AL. Comment on 'thermal boundary resistance of mechanical contacts between solids at sub-ambient temperatures'. J Phys D Appl Phys 2001;34(18):2932–4. https://doi.org/10.1088/0022-3727/34/18/401.

[12] Mamiya T, Yano H, Uchiyama T, Inoue S, Miura Y. Thermal contact of joints between different kinds of metals at low temperatures. Rev Sci Instrum 1988;59(8):1428–30. https://doi.org/10.1063/1.1139684.

[13] Van Sciver SW, Nilles MJ, Pfotenhauer J. Thermal and electrical contact conductance between metals at low temperatures. In: Proceedings of the space cryogenics workshop, Berlin, Germany; 1984.

[14] Little WA. The transport of heat between dissimilar solids at low temperatures. Can J Phys 1959;37(3):334–49. https://doi.org/10.1139/p59-037.

[15] Swartz ET, Pohl RO. Thermal boundary resistance. Rev Modern Phys 1989;61(3):605–68. https://doi.org/10.1103/RevModPhys.61.605.

[16] Prasher RS, Phelan PE. Microscopic and macroscopic thermal contact resistances of pressed mechanical contacts. J Appl Phys 2006;100(6). https://doi.org/10.1063/1.2353704.

[17] Wexler G. The size effect and the non-local Boltzmann transport equation in orifice and disk geometry. Proc Phys Soc 1966;89(4):927–41. https://doi.org/10.1088/0370-1328/89/4/316.

[18] Gundrum BC, Cahill DG, Averback RS. Thermal conductance of metal-metal interfaces. Phys Rev B - Condens Matter Mater Phys 2005;72(24):1–5. https://doi.org/10.1103/PhysRevB.72.245426.

[19] Madhusudana CV. Thermal contact conductance. Springer International Publishing; 2014. p. 9–54 [chapters 2 and 3].

[20] Yoshino Y, Iwabuchi A, Onodera R, Chiba A, Katagiri K, Shimizu T. Vickers hardness properties of structural materials for superconducting magnet at cryogenic temperatures. Cryogenics 2001;41(7):505–11. https://doi.org/10.1016/S0011-2275(01)00118-7.

[21] Cooper MG, Mikic BB, Yovanovich MM. Thermal contact conductance. Int J Heat Mass Transfer 1969;12(3):279–300. https://doi.org/10.1016/0017-9310(69)90011-8.

[22] Yovanovich MM. Thermal contact correlations. In: Horton TE, editor. AIAA paper no. 81-1164; also Progress in aeronautics and aerodynamics: spacecraft radiative transfer and temperature control, vol. 83; 1982. p. 83–95.

[23] Tien C. A correlation for thermal contact conductance of nominally-flat surfaces in a vacuum. In: Flynn D, Peavy B, editors. Thermal conductivity, proceedings of the seventh conference. National Bureau of Standards Special Publication; 1968. p. 755–9.

[24] Mikić BB. Thermal contact conductance- theoretical considerations. Int J Heat Mass Transfer 1974;17(2):205–14. [reference 9 therein]. https://doi.org/10.1016/0017-9310(74)90082-9.

[25] Mikić BB, Rohsenhow WM. Thermal contact conductance, TR 4542-41. NASA contract NR 22-009-065; Sept 1966.

[26] Dhuley RC, Geelhoed MI, Thangaraj JCT. Thermal resistance of pressed contacts of aluminum and niobium at liquid helium temperatures. Cryogenics 2018;93:86–93https://doi.org/10.1016/j.cryogenics.2018.06.003.

[27] Kittel C. Introduction to solid state physics. 8th ed. John Wiley and Sons Inc; 2005.

[28] Antonetti VW, Yovanovich MM. Enhancement of thermal contact conductance by metallic coatings: theory and experiment. ASME J Heat Transfer 1985;107:513–9. https://doi.org/10.1115/1.3247454.

[29] Cryogenic thermal conductivity of OFHC copper, available from NIST at https://trc.nist.gov/cryogenics/materials/OFHC%20Copper/OFHC_Copper_rev1.htm [last accessed 3/27/2019].

[30] Lounasmaa OV. Experimental principles and methods below 1 K. Academic Press; 1974.

[31] Berman R. Some experiments on thermal contact at low temperatures. J Appl Phys 1956;27(4):318–23. https://doi.org/10.1063/1.1722369.

[32] Berman R, Mate CF. Thermal contact at low temperatures. Nature 1958;182:1661–3. https://doi.org/10.1038/1821661a0.

[33] Suomi M, Anderson AC, Holmström B. Heat transfer below 0.2°K. Physica 1968;38(1):67–80. https://doi.org/10.1016/0031-8914(68)90062-1.

[34] Salerno LJ, Kittel P, Spivak AL. Thermal conductance of pressed copper contacts at liquid helium temperatures. AIAA J 1984;22(12):1810–6. https://doi.org/10.2514/3.8856.

[35] Nilles MJ. Thermal and electrical contact resistance of OFHC Cu from 4 K to 290 K. PhD thesis. Univ. Wisconsin Madison; 1986.

[36] Sunada K, Kang Y. Experimental study on thermal contact conductance at liquid helium temperature. In: Proceedings of the sixteenth international cryogenic engineering conference/international cryogenic materials conference; 1997. p. 629–32.

[37] Kerr AR, Horner N. The low temperature thermal resistance of high purity copper and bolted copper joints. Electronics Division Technical Note No. 163. National Radio Astronomy Observatory; 1991.

[38] Bintley D, Woodcraft AL, Gannaway FC. Millikelvin thermal conductance measurements of compact rigid thermal isolation joints using sapphire-sapphire contacts, and of copper and beryllium-copper demountable thermal contacts. Cryogenics 2007;47:333–42. https://doi.org/10.1016/j.cryogenics.2007.04.004.

[39] Kittel P, Spivak AL, Salerno LJ. Thermal conductance of gold plated metallic contacts at liquid helium temperatures. Adv Cryogenic Eng 1992;37(1):241–8.

[40] Schmitt RL, Tatkowski G, Ruschman M, Golwala S, Kellaris N, Daal M, et al. Thermal conductance measurements of bolted copper joints for SuperCDMS. Cryogenics 2015;70:41–6. https://doi.org/10.1016/j.cryogenics.2015.04.006.

[41] Dillon A, McCusker K, Van Dyke J, Isler B, Christiansen M. Thermal interface material characterization for cryogenic electronic packaging solutions. IOP Conf Series: Mater Sci Eng 2017;278. https://doi.org/10.1088/1757-899X/278/1/012054.

[42] Didschuns I, Woodcraft AL, Bintley D, Hargrave PC. Thermal conductance measurements of bolted copper to copper joints at sub-Kelvin temperatures. Cryogenics 2004;44:293–9. https://doi.org/10.1016/j.cryogenics.2003.11.010.

[43] Dhuley RC, Hollister MI, Ruschman MK, Martin LD, Schmitt RL, Tatkowski GL, Bauer DA, Lukens PT. Thermal conductance modeling and characterization of the SuperCDMS SNOLAB sub-Kelvin cryogenic system. IOP Conf Series: Mater Sci Eng 2017;278. https://doi.org/10.1088/1757-899X/278/1/012157.

[44] Boughton RI, Brubaker NR, Sarwinski RJ. Solderless thermal connector for use at low temperatures. Rev Sci Instrum 1967;38:1177–8. https://doi.org/10.1063/1.1721058.

[45] Blondelle F, Sultan A, Collin E, Godfrin H. Electrical conductance of bolted copper joints for cryogenic applications. J Low Temp Phys 2014;175:877–87. https://doi.org/10.1007/s10909-014-1142-4.

[46] Okamoto T, Fukuyama H, Ishimoto H, Ogawa S. Electrical resistance of screw-

fastened thermal joints for ultra-low temperatures. Rev Sci Instrum 1990;61:1332–11134. https://doi.org/10.1063/1.1141184.
[47] Noterdaeme J. Demountable resistive joint for high current superconductors. MS thesis. Massachusetts Institute of Technology; 1978.
[48] Muething K, Ihas GG, Landau J. Metallic thermal connectors for use in nuclear refrigeration. Rev Sci Instrum 1977;48:906–9. https://doi.org/10.1063/1.1135130.
[49] Manninen M, Zimmermann W. On the use of screw-fastened joints for thermal contact at low temperatures. Rev Sci Instrum 1977;48(12):1710–1. https://doi.org/10.1063/1.1134936.
[50] Lau KM, Zimmermann W. Screw-fastened joints for thermal contact at low temperatures. Rev Sci Instrum 1979;50(2):254–5. https://doi.org/10.1063/1.1135782.
[51] Deutsch M. Thermal conductance in screw-fastened joints at helium temperatures. Cryogenics 1979;19(5):273–4. https://doi.org/10.1016/0011-2275(79)90141-3.
[52] Accuracy of Lakeshore Cernox thermometers taken from https://www.lakeshore.com/products/cryogenic-temperature-sensors/cernox/models/pages/Specifications.aspx [last accessed 3/27/2019].
[53] Bernat TP, Alexander NB, Kaae JL. Thermal and electrical conductivities of electroplated gold. Fusion Sci Technol 2007;51(4):782–5https://doi.org/10.13182/FST07-A1479.
[54] Yovanovich MM. Micro and macro hardness measurements, correlations, and contact models. In: 44th AIAA aerospace sciences meeting and exhibit, AIAA 2006-979; 2006 (https://doi.org/10.2514/6.2006-979).
[55] Hasselström A, Nilsson U. Thermal contact conductance in bolted joints. MS Dissertation. Gothenburg, Sweden: Chalmers University of Technology; 2012 [reference 22 therein].
[56] Coefficients of friction taken from http://www-eng.lbl.gov/~ajdemell/coefficients_of_friction.html [last accessed 3/27/2019].